Molecular Vision 2022; 28:317-330 <http://www.molvis.org/molvis/v28/317>
Received 20 December 2021 | Accepted 28 September 2022 | Published 1 October 2022

Structural and functional analysis of SNP rs76740365 G>A in exon-3 of the alpha A-crystallin gene in lens epithelial cells

Zhennan Zhao,[1,3] Yang Sun,[1,3] Qi Fan,[1,3] Yongxiang Jiang,[1,3] Yi Lu[1,3]

(The first three authors contributed equally to this work.)

[1]Department of Ophthalmology and Vision Science, Eye Ear Nose and Throat Hospital of Fudan University, Shanghai, China; [2]NHC Key Laboratory of Myopia (Fudan University), Laboratory of Myopia, Chinese Academy of Medical Sciences, Shanghai, China; [3]Key Laboratory of Visual Impairment and Restoration of Shanghai, Shanghai, China

Purpose: To clarify the effect of a previously identified single nucleotide polymorphism (SNP; rs76740365 G>A) in the exon-3 of the *alpha A-crystallin (CRYAA)* gene on the properties of *CRYAA* and to investigate its function in human lens epithelial cells (HLECs).

Methods: The human recombinant wild-type and mutant *CRYAA* (E156K) were constructed, and the molecular weight was measured by mass spectrometry. The structural changes induced by E156K mutation were analyzed by UV circular dichroism spectra and intrinsic tryptophan fluorescence and were predicted using Schrödinger software. The chaperone-like ability of wild-type and E156K mutant *CRYAA* was invested against the heat-induced aggregation of βL-crystallin and the DTT-induced aggregation of insulin. HLECs expressing wild-type and mutated *CRYAA* were subjected to quantitative PCR (qPCR) and western blot. Cell apoptosis was determined using flow cytometry analysis, and the expression of apoptosis-related proteins were determined using western blot.

Results: The mass spectrometric detection revealed that E156K mutation had no significant effect on the apparent molecular mass of the *CRYAA* oligomeric complex. Evaluation of the structures of the *CRYAA* indicated that E156K mutation did not significantly affect the secondary structures, while causing perturbations of the tertiary structure. The mutant *CRYAA* displayed an increase in chaperone-like activity, which might be related to the increase of the surface hydrophobicity. We also predicted that E156K mutation would induce a change from negatively charged surface to positively charged, which was the possible reason for the disturbance to the surface hydrophobicity. Transfection studies of HLECs revealed that the E156K mutant induced anti-apoptotic function in HLECs, which was possibly associated with the activation of the p-AKT signal pathway and downregulation of Casepase3.

Conclusions: Taken together, our results for the first time showed that E156K mutation in *CRYAA* associated with ARC resulted in enhanced chaperone-like function by inducing its surface hydrophobicity, which was directly related to the activation of its anti-apoptotic function.

Age-related cataract (ARC) remains the leading cause of visual impairment worldwide, as well as the largest contributor to blindness in adults 50 years of age and older [1,2]. At present, surgical removal of the opaque lens is the primary therapy for restoring sight in cataract patients. However, the mechanism involved in the cataractogenesis and the process of ARC have not been fully elucidated, and there is no proven method of prevention for cataract.

Alpha A-crystallin (CRYAA) is the main protein in the lens, playing a crucial role in maintaining lens transparency and constituting approximately 35% of all lens crystallins. As a molecular chaperone and a member of the small heat-shock protein family, *CRYAA* helps maintain the solubility of the other lens proteins, such as β- and γ-crystallins, and protects them from aggregation. *CRYAA*-knockout mice display a small lens, lens epithelial cell death, reduced proliferation, cataract, and inhibition of pathological neovascularization [3]. Previous studies have demonstrated that the levels of *CRYAA* were decreased in the nuclear capsules of ARC patients [4-6] compared to those of controls, while the mechanisms underlying the downregulation of *CRYAA* in the lens have remained unclear.

CRYAA is involved in multiple cellular functions, including apoptosis and cell migration. However, mutations in *CRYAA* can detrimentally affect such function. To date, numerous genetic variants have been identified in the *CRYAA* gene, the majority of which are single nucleotide polymorphisms (SNPs). Bhagyalaxmi et al. reported an association of G>A transition found in exon-1 of the *CRYAA* gene with ARC and differential risk of genotypes for individual types

Correspondence to: Yi Lu, Eye Institute and Department of Ophthalmology, Eye & ENT Hospital, Fudan University, Shanghai, 200031, China; Phone: 86-21-64377134; FAX: 86-21-64377151; email: luyieent@126.com

of cataracts [7]. In the exon-2 of the *CRYAA* gene, the F71L mutation resulted in defective chaperone-like function, intimately linked to ARC [8]. The SNP rs727846 in the *CRYAA* gene has been reported to be related to ARC through decreasing the transcriptional activity of the *CRYAA* promoter [9]. Our previous study revealed that SNPs identified in the 5′ untranslated region (5′ UTR) of *CRYAA* were associated with susceptibility to ARC, especially the nuclear subtype, in a Han Chinese population [10].

Recently, our team found that the SNP (rs76740365 G>A) in the exon-3 of the *CRYAA* gene is closely involved in cataract formation, especially posterior subcapsular cataract (PSC; Chen JH et al., unpublished data). The mutation in rs76740365 is a missense mutation that causes the amino acid substitution from glutamic acid (E) to lysine (K), which localizes in the 156th amino acid residues of *CRYAA*. However, its functional role in the pathogenesis of ARC remains unclear. In the present study, we aimed to further elucidate the underlying mechanism of E156K mutation in causing cataract at the molecular and cellular levels.

METHODS

Expression of wild-type and mutant αA-crystallin and purification: In the present work, cDNA encoding human *CRYAA* was cloned into a pSmart-I vector (Invitrogen) and used as a template to generate the E156K mutation in the *CRYAA* gene using a quick-change site-directed mutagenesis kit (Stratagene, La Jolla, CA). The E156K mutation was confirmed by automated DNA sequencing. The pSmart-I plasmids were introduced into *Escherichia coli* BL21 (DE3) for protein expression using IPTG. The recombinant proteins of wild-type and E156K *CRYAA* were purified using a Superdex G200 gel filtration column (GE Healthcare, Little Chalfont, UK). The homogeneity of purified protein was identified by SDS–PAGE and immunodetection as described previously [11].

MALDI-TOF mass spectrometry: The mass spectrometric analysis was performed using a Brucker BIFLEX matrix-assisted laser desorption time-of-flight (MALDI-TOF) mass spectrometer. A saturated solution of 10 mg/mL of sinapinic acid in 50% acetonitrile/water containing 0.1% trifluoroacetic acid was used as the matrix. About 1 µl volume of sample solution and the matrix solution at a ratio of 1:1 were applied to the MALDI target plate and air dried. Mass spectra were obtained in a linear mode and generated using Flex-control 99 Software (Bruker Daltonics, Bremen, Germany). Finally, all acquired spectra were processed with Flex Analysis v.3.3 (Bruker Daltonics).

Circular dichroism (CD) measurements: The secondary and tertiary structure of αA-crystallin was examined by far-UV and near-UV CD spectra at 25 °C in a Jasco-810 spectropolarimeter (Jasco, Inc., Japan). Spectra were recorded using a bandwidth of 1 nm at a scanning speed of 200 nm/min. Far-UV CD spectra were collected from 195 to 250 nm in a 1 mm pathlength quartz cuvette, and near-UV spectra were collected from 250 to 300 nm in a 10 mm pathlength quartz cuvette. Protein concentrations of 0.2 mg/ml and 1 mg/ml in 10 mM phosphate buffer at pH 7.2 were used for recording the far- and near-UV CD spectra, respectively. The reported spectra were an average of five accumulations, and the data were analyzed using CDNN (circular dichroism analysis using neural networks) software.

Fluorescence measurements: The fluorescence measurements were recorded using a fluorescence spectrophotometer (RF-6000, Shimadzu, Japan). The selective tryptophan excitation wavelength was set at 295 nm, and the emission was collected in the range of 200–400 nm using 5-nm/5-nm slits. The hydrophobic probe, 4,4′-Bis-1-anilino naphthalene 8-sulfonate (bis-ANS; Molecular Probes, Eugene, OR), was used to check the surface hydrophobicity of proteins. Bis-ANS emission spectra were detected using an excitation wavelength of 395 nm, and spectra were recorded from 200 to 560 nm using 5-nm/5-nm slits. Three scans were averaged, and buffer spectra were subtracted from protein spectra to calculate each spectrum.

Structural modeling: Protein structural modeling was performed using Maestro molecular modeling software (Schrödinger, LLC, New York, NY) [12]. The structural graphics were prepared using PyMOL Molecular Graphics System software (Version 1.3 Schrödinger, LLC).

The chaperone-like function of wild-type and mutant human αA-crystallin: The chaperone-like ability of wild-type and E156K mutant *CRYAA* was invested against the heat-induced aggregation of βL-crystallin and the DTT-induced aggregation of insulin. Aggregation was monitored by measuring light scattering at 360 nm using the Biotek microplate reader (BioTek ELX800 Absorbance Microplate Reader, BioTek Instruments, Colmar, France) according to previously described methods [8,13].

Cell culture and transfection: The human lens epithelium (HLE) SRA01/04 cells (ATCC; Rockville, MD) were maintained in Dulbecco's modified eagle medium (DMEM) containing 20% fetal bovine serum (FBS) at 37 °C in a humidified 5% CO_2 incubator. For transfection, cells were seeded into six-well plates 24 h before and grown to 70%–80% confluence. The transfection mixture consisting of 2 µg of plasmid DNA and 4 µl Lipofectamine™ 2000

(Invitrogen) reagent in 2 ml of serum-free medium was then added to a six-well plate. Transfected cells were incubated at 37 °C in CO_2 for 48 h before use.

Establishment of stable CRYAA knockdown cell lines: To knock down the endogenous *CRYAA*, shRNAs targeting four unique sequences were constructed (sh1–sh4) using the lentiviral vector PHY-310. The target sequences were as follows: human CRYAA sh1, GGG ACA AGT TCG TCA TCT TCC; human CRYAA sh2, GCA GGA CGA CTT TGT GGA GAT; human CRYAA sh3, CCG GCA TCT CTG AGG TTC GAT; human CRYAA sh4, CCT CGT CCT AAG CAG GCA TTG. Selection of infected cells was done with puromycin (2 μg/ml). The knockdown efficiency of the shRNA candidates was measured by quantitative PCR (qPCR).

Plasmid construction: The human *CRYAA* was amplified using primers, as described above, and inserted into the PHY-LV-OE1.6-FLAG vector (Invitrogen) using the restriction enzymes Hind III and KpnI (Takara). The rs76740365 SNP mutant of *CRYAA (*E156K*)* was generated by site-directed mutagenesis.

Western blot: For western blots, cells were lysed in radioimmunoprecipitation assay (RIPA) lysis buffer (R0278, Sigma, St Louis, MO) supplemented with protease inhibitor cocktail (#78425, Thermo Scientific, Rockford, IL). The lysate was centrifuged at 12,000 × *g* for 15 min at 4 °C, and the supernatant was collected and stored for further analysis. To ensure equal protein load, protein concentration was measured using a bicinchoninic acid (BCA) assay. The protein samples were then denatured by boiling at 100 °C for 5 min in 5X loading buffer containing 10% SDS and 100 mM dithiothreitol. Equal amounts of protein were separated on 10% sodium dodecyl sulfate PAGE (SDS–PAGE) before being electrotransferred to 0.45-μm pore-size polyvinylidene difluoride (PVDF) membranes (IPVH00010, Merck, Burlington, MA). After blocking with 5% nonfat milk prepared in tris-buffered saline with 0.1% Tween (TBS-T) for 1 h at room temperature, the PVDF membranes were probed overnight with the following primary antibodies at 4 °C: CRYAA (ab181866, Abcam, Cambridge, MA), β-actin (A3854; Sigma), AKT (#9272; CST, Ipswich, MA), p-AKT(#4060; CST), Caspase 3 (#9662; CST), and Caspase 9 (#9502; CST). The next day, the membranes were washed with TBS-T three times for 10 min and incubated with peroxidase-conjugated goat anti-mouse IgG (H^+L) or anti-rabbit IgG (H^+L; Yeasen, China) for 1 h. Signals were visualized by Super Signal West Pico (NCI5079, Thermo Scientific). Images from western blotting experiments were processed using a Kodak Imaging System and quantitated using the ImageJ program.

Quantitative real-time PCR (qRT-PCR): RNA isolation and qRT-PCR analysis were performed as previously described [14]. Total RNA was isolated TRIzol (15,596, Thermo Fisher, Waltham, MA) and quantified on NanoDrop 2000 (Thermo Fisher). The extracted RNA was transcribed into cDNA using a reverse transcription kit (KR106–02, Tiangen, China), and the expression of *CRYAA* was determined using SYBR Premix (FP205–02, Tiangen) on an ABI 7500 PCR machine following the manufacturer's manual. The following sequences of primer pairs are described below: CRYAA, 5′-CTG AGG ACG ATG TGT CTA ACC TC −3′ (forward) and 5′- AGG CCT GGA CTC AGC TGA −3′ (reverse); β-actin, 5′- TTG TTA CAG GAA GTC CCT TGC C −3′ (forward) and 5′- ATG CTA TCA CCT CCC CTG TGT G −3′ (reverse).

Apoptosis: Cell apoptosis was determined using an Annexin V-fluorescein isothiocyanate (FITC) and propidium iodide (PI) apoptosis detection kit (Beyotime, Shanghai, China). After the indicated treatments, the cells were collected through trypsinization, followed by washing twice with PBS. For analysis of apoptosis, the human lens epithelial cells (HLECs) were stained with Annexin V-FITC for 15 min at room temperature and then incubated with PI on ice. After incubation, all samples were analyzed by flow cytometry (BD Biosciences, Franklin Lakes, NJ, USA). Cells stained positive with Annexin V and negative with PI were considered as early apoptosis.

Statistical analysis: All experiments were repeated three times independently with similar results, and the data were shown as mean ± standard deviation (SD). Significant differences were assessed using the two-tailed Student *t* test, ANOVA two-way test with Bonferroni post-test, or Fisher's exact test, depending on the types of variables. The statistical analysis and the calculation of odds ratios (ORs) were conducted using SPSS for Windows, version 17.0 (SPSS, IBM Inc., Chicago, IL). The SHEsis software platform was used to estimate the Hardy–Weinberg equilibrium (HWE), linkage disequilibrium (LD), and haplotype frequencies [15]. Differences were considered statistically significant at p values < 0.05.

RESULTS

Effect of E156K mutation on the molecular mass of CRYAA: To characterize the structural significance of the E156K mutation, we cloned both wild-type (WT) and mutant genes expressed in *E. coli*. The mutant proteins were purified as described for WT, and the SDS–PAGE profile of WT and E156K mutant proteins after purification and homogeneity of recombinant *CRYAA* are shown in Figure 1. The molecular mass of E156K *CRYAA* was then determined using the

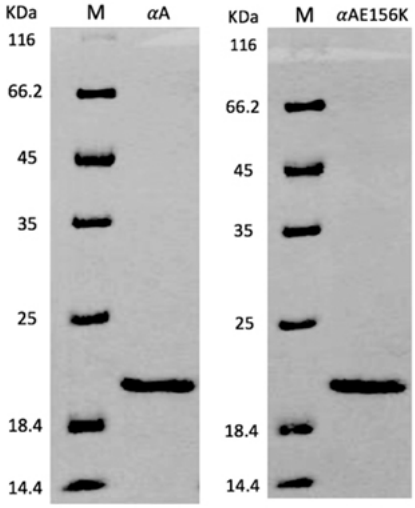

Figure 1. SDS-PAGE of purified wild-type CRYAA and E156K CRYAA. **A**: wild-type CRYAA. **B**: E156K CRYAA. M represents molecular weight marker. Lane αA represents wild-type αA-crystallin and Lane αA E156K represents recombinant mutant αA-crystallin.

MALDI-TOF mass spectrometer (Figure 2). Mass spectrometry analysis showed similar molecular weight both for the mutant and wild-type proteins, indicating insignificant differences in the molecular masses (Table 1).

Secondary structural changes induced by E156K mutant in CRYAA: To determine the secondary structure of WT and E156K mutant *CRYAA*, two proteins were analyzed using far-UV circular dichroism (CD) spectroscopy. As shown in Figure 3, both the WT and mutant proteins showed a characteristic minimum around 217 nm, which was indicative of a β-sheet structure. The CDNN analysis of the CD data revealed that E156K *CRYAA* possessed increased β-sheet content with a concomitant decrease in α-helix compared to WT *CRYAA*, while differences in α-helix and β-sheet content between the two proteins were not significant (Table 2). These results suggest that E156K mutation has no significant effect on the secondary structure of *CRYAA*.

Tertiary structural changes induced by E156K mutant in CRYAA: The near-UV CD spectra of proteins reflect differences in conformation and can be used to probe the tertiary structures of proteins [16,17]. In our study, the near-UV spectrum of WT proteins exhibited different peaks beyond 260 nm and 277 nm from E156K mutant protein, suggesting an alteration in the signal for tryptophan in the 270–290 nm region and phenylalanine in the 250–270 nm region in the E156K mutant compared to the WT protein (Figure 4A). To further corroborate the findings from the near-UV spectrum, the tertiary structure alterations were analyzed by tryptophan fluorescence measurements (Figure 4B). The WT and mutant *CRYAA* did not show any variation in emission maxima of tryptophan fluorescence. However, the fluorescence intensity decreased in mutant proteins, indicating a potential alteration of the microenvironment of aromatic amino acid residue in mutant proteins when compared to WT proteins. Taken together, the results revealed that E156K mutation was likely to affect the tertiary structure.

Surface hydrophobicity: To evaluate the surface hydrophobicity of WT and mutation proteins, Bis-ANS fluorescence was employed and showed that the fluorescence emission peak position was similar for both proteins (Figure 5). However, the fluorescence intensity of bis-ANS was found to be slightly higher for the mutant protein compared to the WT protein, a difference indicating an increase in exposed hydrophobic sites or positively charged residues in E156K mutant *CRYAA*. To understand the structural features that contribute to the increased surface hydrophobicity of E156K *CRYAA*, we performed molecular modeling on the WT and mutant proteins. The model of dimer structure illustrated that E156K mutation induced a clear change in the protein structure (Figure 6). As a result, their negatively charged surface changed to positively charged, which was in good agreement with the increase in the bis-ANS fluorescence intensity of E156K *CRYAA*.

Chaperone activity of E156K mutant CRYAA: We further detected the chaperone-like activity (CLA) of *CRYAA* in two proteins using DTT-induced aggregation of insulin and the heat-induced aggregation of βL-crystallin as model systems (Figure 7). In DTT-induced aggregation of insulin, the CLA of E156K mutant protein was increased by approximately 15.62% compared to WT. Similarly, the E156K mutant showed about 9.35% higher CLA in the heat-induced aggregation of βL-crystallin compared to WT *CRYAA*. These

Table 1. Molecular weights of wild-type αA-crystallin and E156K mutant αA-crystallin.

Proteins	m/z	Intensity	Mass
αA	20054.43	2852.25	20053.42
αA E156K	20053.59	3012.43	20052.583

findings suggest that E156K mutation leads to an increase in the chaperone activity of *CRYAA*.

Bioinformatics functional analysis proteins interacting with CRYAA: In our previous study, a total of 343 proteins interacting with *CRYAA* were identified by using protein microarrays [18]. To further investigate the functions of these proteins, we performed protein chip enrichment analysis and found 143 proteins that were significantly different. Next, gene ontology (GO) enrichment analysis was performed using DAVID Bioinformatics Resources [19,20] to obtain a biologic view of these differentially expressed proteins, and the protein–protein interaction network was constructed according to the functional relationships annotated in the KEGG database. The results revealed that the proteins interacting with *CRYAA* were related to chaperone, hydroxylase, proliferation, and transcription regulation (Figure 8).

E156K mutant CRYAA induced anti-apoptotic function and activated the AKT signaling pathway in HLECs: The bioinformatics functional analysis of proteins interacting with *CRYAA* showed enrichment for proteins that were

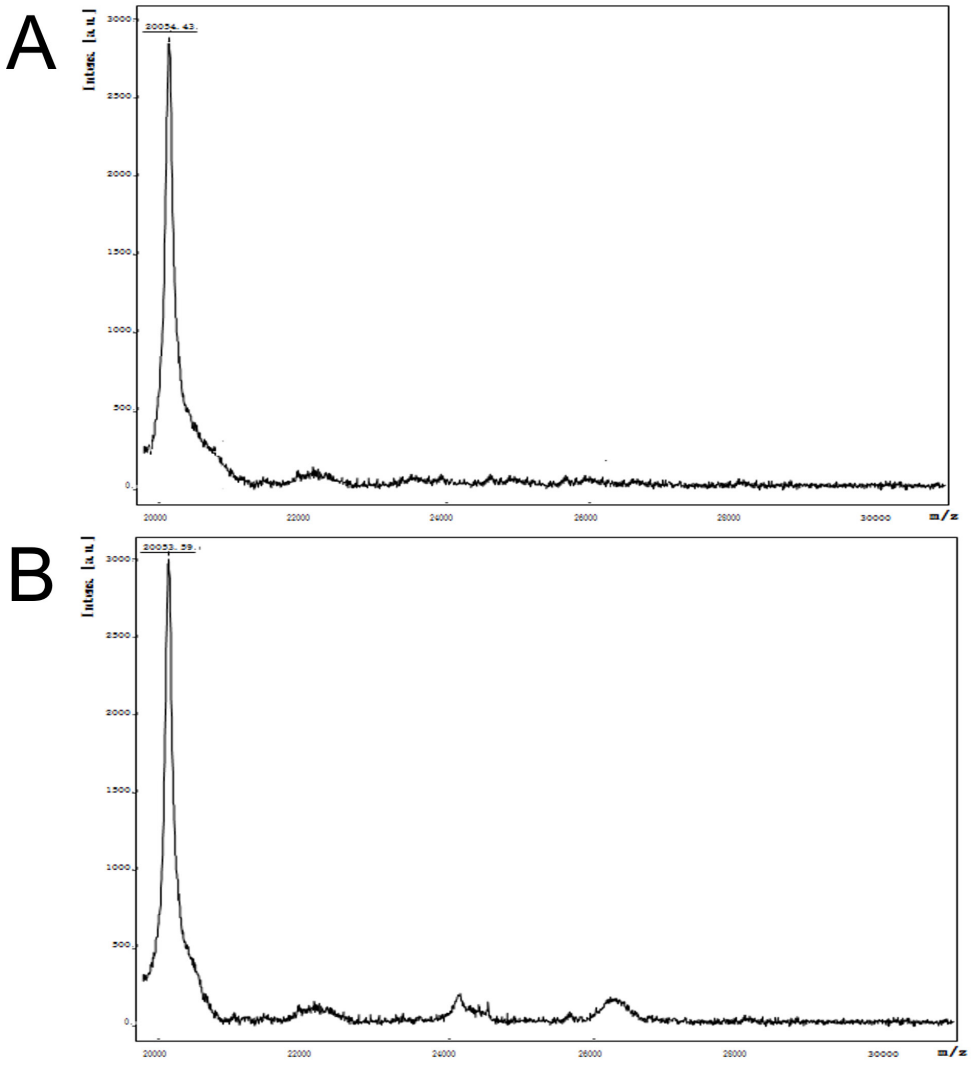

Figure 2. Mass spectrometry of wild-type and E156K CRYAA. **A**: wild-type CRYAA. **B**: E156K CRYAA.

Table 2. Percent secondary structure content in wild type and E156K αA-crystallin.

Protein	α-helix	β-sheet	β-turn	Radom coil
αA	24.40%	38.70%	18.30%	35.90%
αA E156K	22.20%	41.90%	18.90%	35.40%

associated with apoptosis, such as AKT. Furthermore, to investigate the cellular apoptosis induced by mutant E156K *CRYAA* in HLECs, we knocked down *CRYAA* expression through lentivirus transduction. Figure 9A shows that all four *CRYAA* shRNAs suppressed expression of *CRYAA* protein in HLECs. *CRYAA* knockdown lens epithelial cells (CRYAA-sh1) were selected for further experiments because they had a better inhibitory effect on *CRYAA* expression. Subsequently, we transfected the CRYAA-sh1 HLECs with WT *CRYAA* plasmid or *CRYAA* mutant E156K plasmid. As shown in Figure 9B, the expression of *CRYAA* protein in the WT group and the mutant E156K group was higher than that in the vector groups, whereas the level of *CRYAA* protein in the vector group was similar to that in the control group.

Cell apoptosis was assessed with annexin V-FITC/propidium iodide staining, and the percentage of apoptotic cells in the HLECs transfected with mutant E156K was less than that in the WT group, indicating that the antiapoptotic effect induced by mutant E156K was stronger than WT *CRYAA* (Figure 10A). AKT/p-AKT and apoptosis-related proteins were then analyzed with a western blot assay (Figure 10B). The expression of p-AKT was elevated in the mutant E156K group, and the opposite results was observed in the expression of casepase-3. Together, mutant E156K *CRYAA* exerted an anti-apoptotic effect in HLECs, associated with the activation of the AKT signal pathway and downregulation of casepase-3.

DISCUSSION

A recent study by our group demonstrated that SNP (rs76740365 G>A) in the *CRYAA* exon region was associated with the susceptibility of ARC, especially posterior subcapsular cataract (PSC), and likely increased the risk of PSC development (Chen et al., unpublished data). This variant has not been reported in the gnomAD database, indicating that it is rare in the general population. Furthermore, in an attempt to gain insight into the structural variations caused by the missense E156K mutation in *CRYAA*, we have constructed, expressed, and purified human recombinant E156K *CRYAA*.

It was observed that E156K mutation did not affect the structure of the proteins in terms of the apparent molecular mass and the secondary structure, while it could alter the tertiary structure, resulting in disturbance to the surface hydrophobicity or surface charge of *CRYAA*. Ito et al. reported that phosphorylation of alpha B-crystallin caused the dissociation of large oligomers to smaller molecules [21]. Other studies have demonstrated that R21C, R54C, and R116H mutations in *CRYAA* are associated with congenital cataracts and have an important effect on molecular weight [22,23]. However, no major difference in molecular weights was found

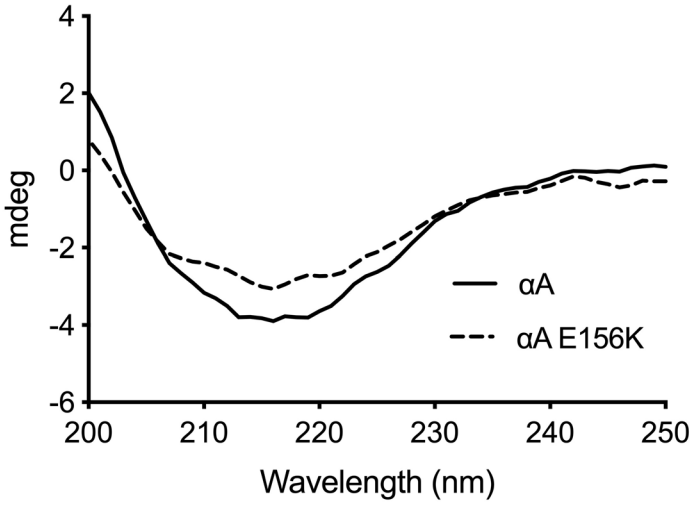

Figure 3. Far-UV CD spectra of wild-type (solid curve) and E156K mutant (dashed curve) *CRYAA*.

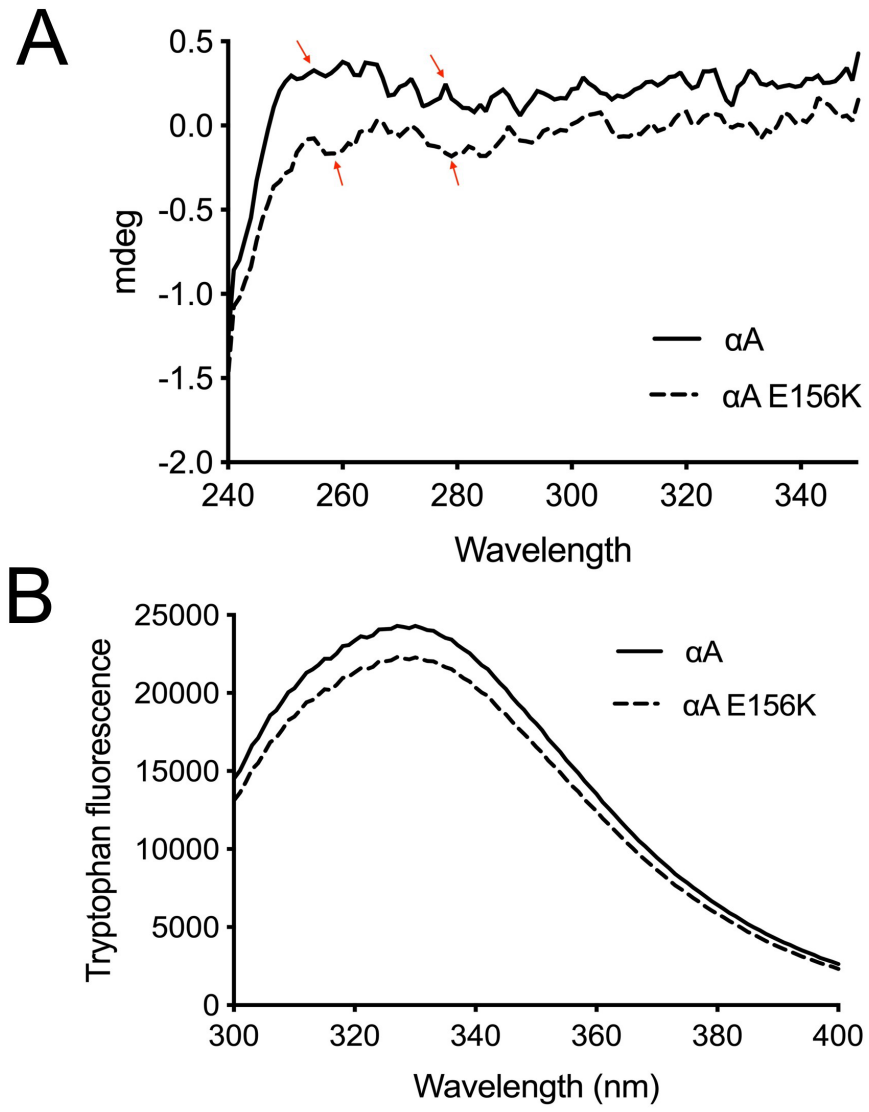

Figure 4. Tertiary structural studies on wild-type and E156K *CRYAA*. Near-UV CD spectra (A) and tryptophan fluorescence spectra (B) of wild-type (solid curve) and E156K mutant (dashed curve). The arrows refer to the peaks beyond 260 nm and 277 nm in the wild-type and E156K *CRYAA* that are different from one another.

in our study, suggesting that the mutation of E156K had no detectable effect on the size of the oligomers. This is possibly because the E156K mutation is located in the short C-terminal regions in *CRYAA*, which are suggested to play an important role in the structure and chaperone activity but have a negligible impact on oligomeric size [24,25]. The results from far-UV measurements indicated that mutant E156K did not perturb the secondary structure of proteins, and all spectra reflected characteristics of the dominant β-sheet structure, which was consistent with previous studies on the structure of wild-type *CRYAA* [26]. In the studies by Validandi et al. and Bhagyalaxmi et al., F71L mutation did not significantly affect the apparent molecular mass, secondary and tertiary structures, and hydrophobicity of *CRYAA* but had a substantial influence on functional properties [8,13]. However, in this study, the Glu156 residue in *CRYAA*, mutated to Lys (K), induced significant alterations in the protein's tertiary structure. Bis-ANS fluorescence was slightly increased in the mutant protein compared to the WT protein, indicating a positive surface charge or exposed hydrophobic surface of E156K *CRYAA*. Meanwhile, the structural model also illustrated a change of surface charge from negative to positive in E156K *CRYAA*. As suggested previously by Farnsworth et al., both charges and hydrophobic surfaces have a significant role in the chaperone activity of α-crystallin subunits as small heat-shock proteins [27]. In addition, hydrophobicity is associated with crystallin activities, and increased hydrophobic interaction could lead to the reduction of solubility

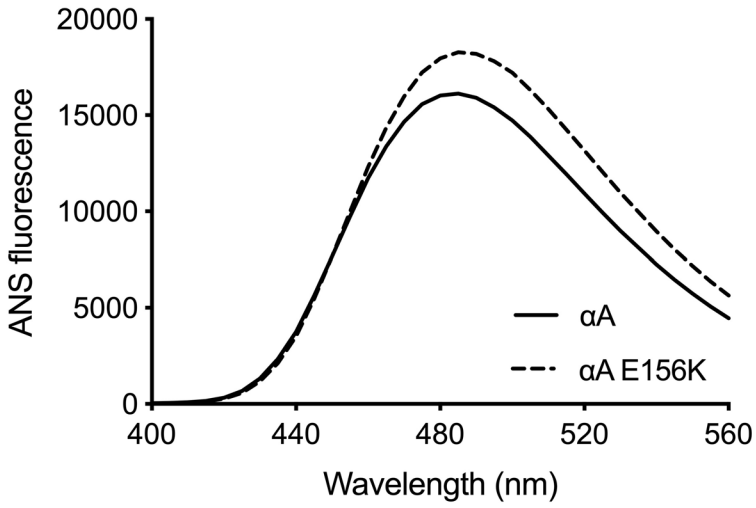

Figure 5. ANS fluorescence spectra of wild-type (solid curve) and E156K mutant (dashed curve).

or abnormal folding, which are suggested in the differences between the mutant and wild-type proteins.

CRYAA acts as a molecular chaperone protecting other crystallins from aggregation or inactivation and traps aggregation-prone denatured proteins. Sharma et al. identified a 19-amino acid peptide sequence from αA-crystallin, which possessed the hydrophobic site and anti-aggregation property, suggesting a critical role for the αA-crystallin domain of heat-shock proteins in the chaperone-like activity [28]. Later, they reported that the residues 70–88 in αA-crystallin prevented

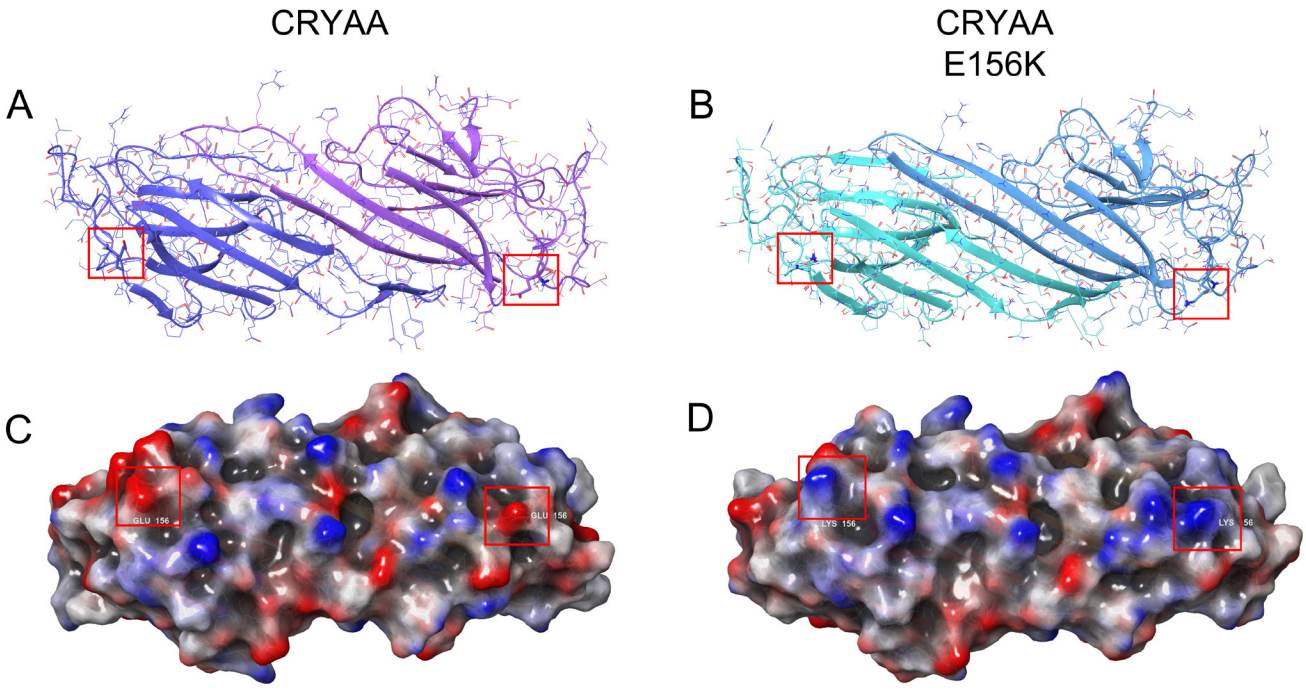

Figure 6. The predicted structure of wild-type CRYAA and E156K CRYAA. **A**: The predicted loop-helix structures of wild-type CRYAA. **B**: The predicted Loop-helix structures of E156K CRYAA. **C**: The predicted surface structures of wild-type CRYAA. **D**: The predicted surface structures of E156K CRYAA. Positively charged residues are colored in blue and negatively charged residues are colored in red. The red box highlights structural differences in the amino acid residues differences between wild-type CRYAA and E156K CRYAA.

the oxidation and UV-induced aggregation of γ-crystallins, further confirming that the polypeptide sequence was indeed a functional element of αA-crystallin, responsible for its chaperone-like property [29]. Previous studies have demonstrated that the decrease in chaperone activity of alpha-crystallin possibly promotes the aggregation of lens proteins, which could eventually lead to cataract formation [30]. However, Biswas et al. reported an enhancement in the chaperone function of α-crystallin due to increased surface hydrophobicity by methylglyoxal (MGO) modification [25]. Others proved that α-dicarbonyl compounds like MGO were the major sources of advanced glycation end-products (AGEs), which accumulate in lenses during the aging process and even more rapidly in cataractous lenses [31,32]. Together, these findings suggested that the development of cataract disease was not necessarily correlated with the decrease in the activity of alpha-crystallin. In our study, E156K mutation markedly enhanced the chaperone function of *CRYAA*. Considering our previous findings that the SNP (rs76740365 G>A) in the exon-3 of the *CRYAA* gene was related to the PSC development, we speculated further that the increased chaperone function of E156K *CRYAA* was probably associated with the pathogenesis of PSC. However, experiments with E156K mutant *CRYAA* are required to fully elucidate the mechanisms by which it is involved in PSC formation in the future.

To further investigate the proteins interacting with *CRYAA* and the potential roles that these protein interactions play in the function of *CRYAA*, we performed a bioinformatics functional analysis. The results revealed that these proteins were associated with chaperone and hydroxylase and involved in the processes of transcription regulation and proliferation. Xi et al. reported slower proliferation and higher apoptosis in *CRYAA*-knockout lens epithelial cells than in wild-type cells, suggesting a role for *CRYAA* in regulating cell proliferation [33]. However, we found no

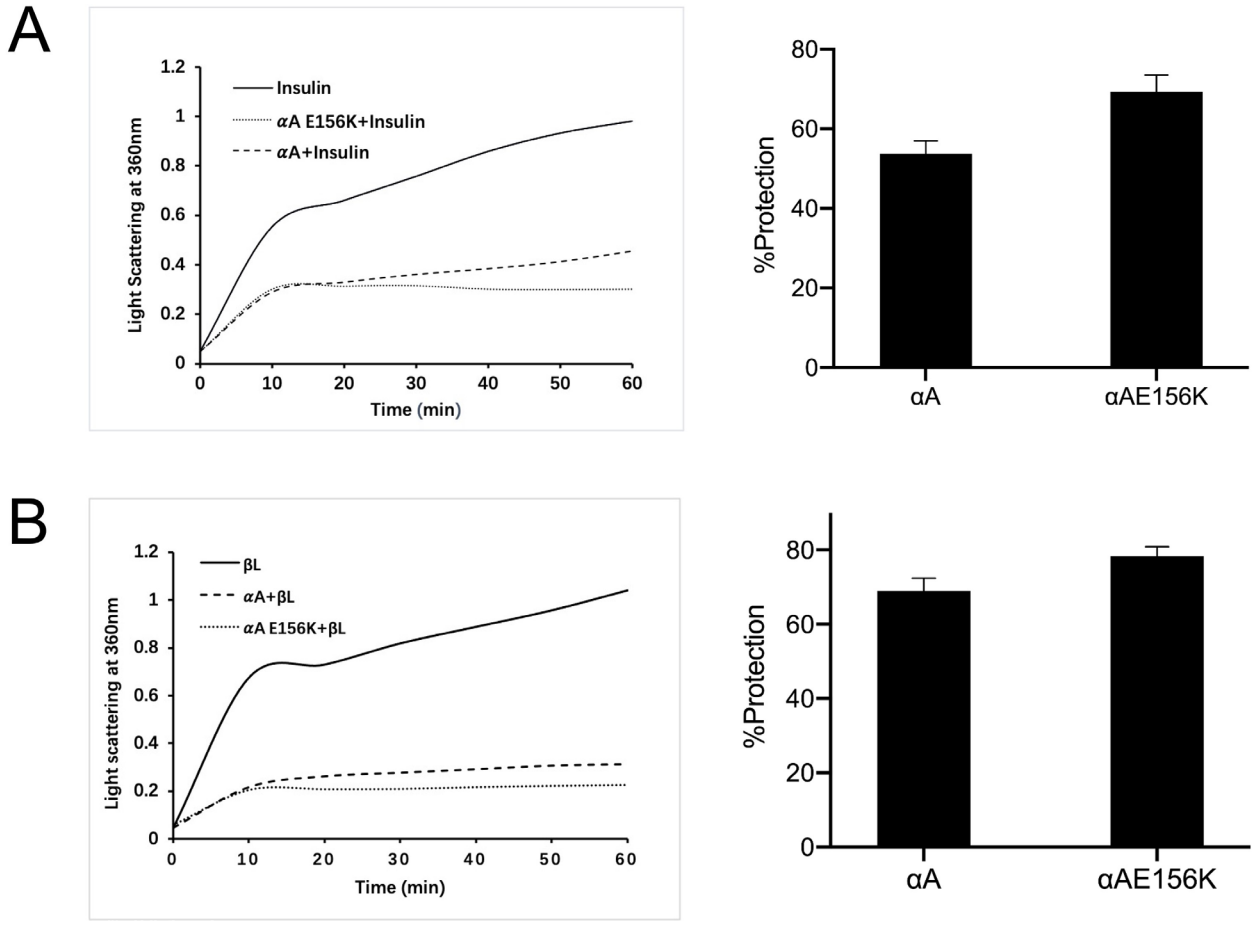

Figure 7. Chaperone-like activity of E156K mutant in CRYAA compared to wild-type CRYAA. **A**: DTT-induced aggregation of insulin. **B**: heat-induced aggregation of βL-crystallin.

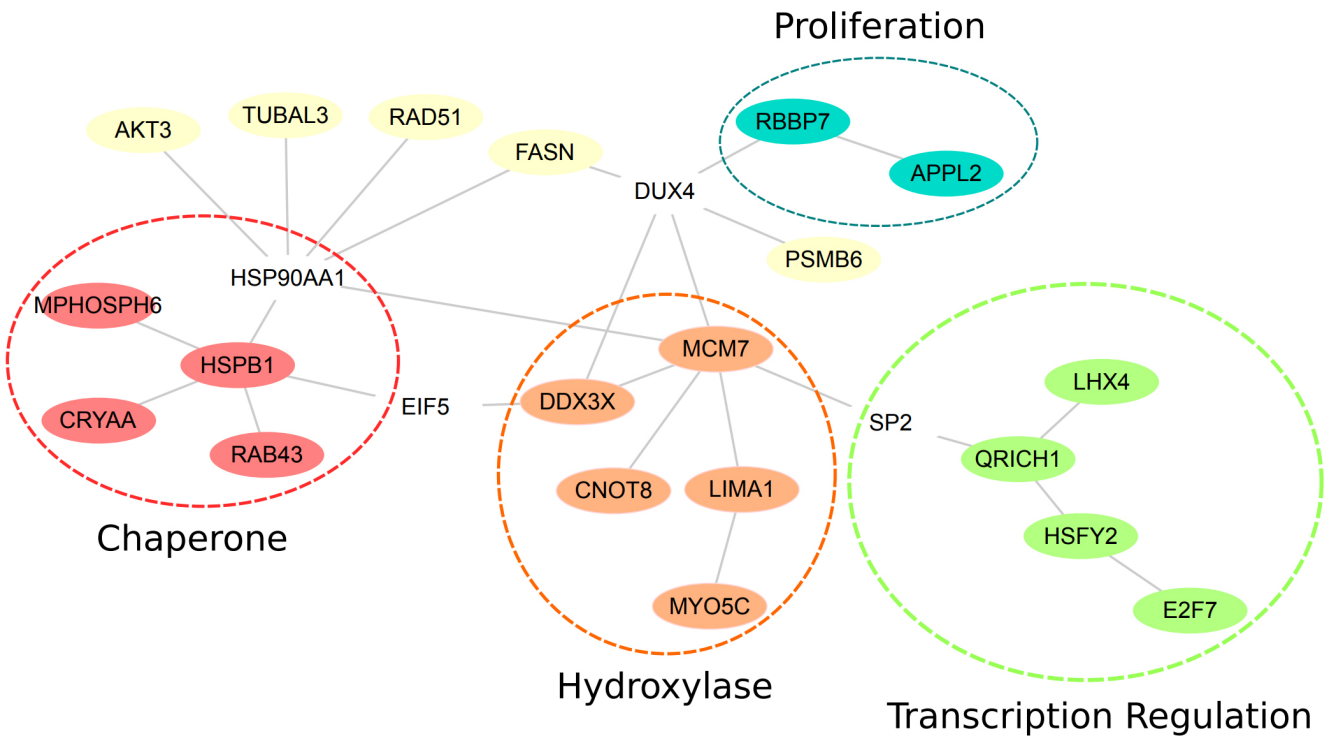

Figure 8. Functional protein association network determined using DAVID Bioinformatics Resources with respect to the target proteins.

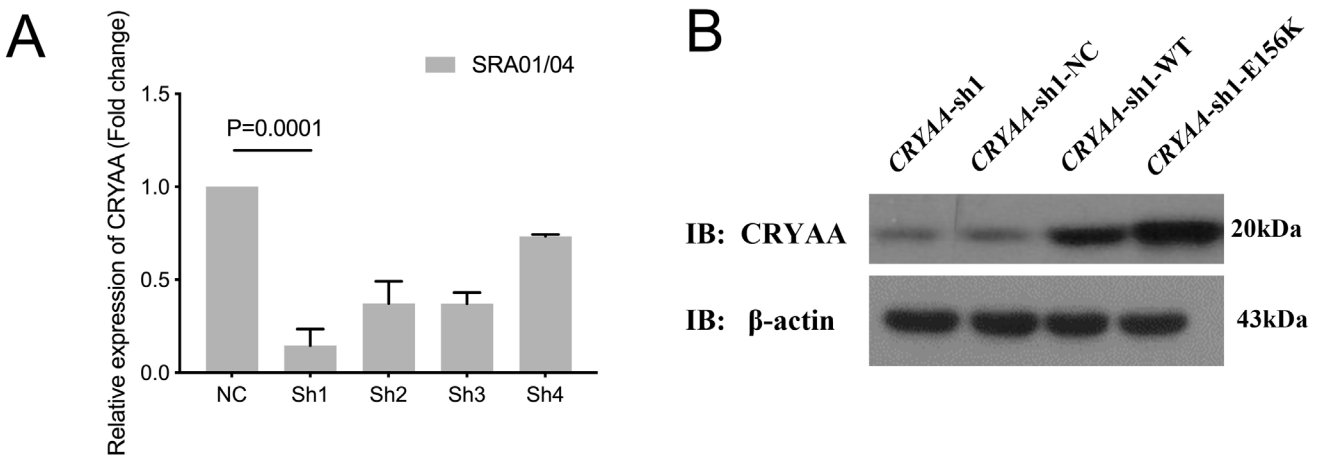

Figure 9. Construction of the CRYAA knock down HLECs. **A**: CRYAA mRNA expression was significantly down-regulated in HLECs transfected with CRYAA-sh1, CRYAA-sh2, CRYAA-sh3 and CRYAA-sh4. **B**: Expression of CRYAA protein was determined with western blot assays and the CRYAA protein expression was significantly up-regulated in CRYAA-sh1 transduced with wild type CRYAA plasmid and CRYAA mutant E156K plasmid.

evidence for aberrant proliferation between wild-type and E156K *CRYAA*, suggesting that E156K mutation in *CRYAA* did not significantly affect cell-proliferation levels (Appendix 1 and Appendix 2). The protein–protein interaction analysis also indicated that *CRYAA* interacted with various proteins that may contribute to its potent antiapoptotic protection against oxidative damage. Our previous study demonstrated that *CRYAA* provided protection against oxidative stress [34].

It is also well known that *CRYAA* comprises distinct anti-apoptotic regulators and prevents stress-induced apoptosis by regulating multiple signaling pathways [35]. In the present study, *CRYAA* induced anti-apoptotic ability in HLECs,

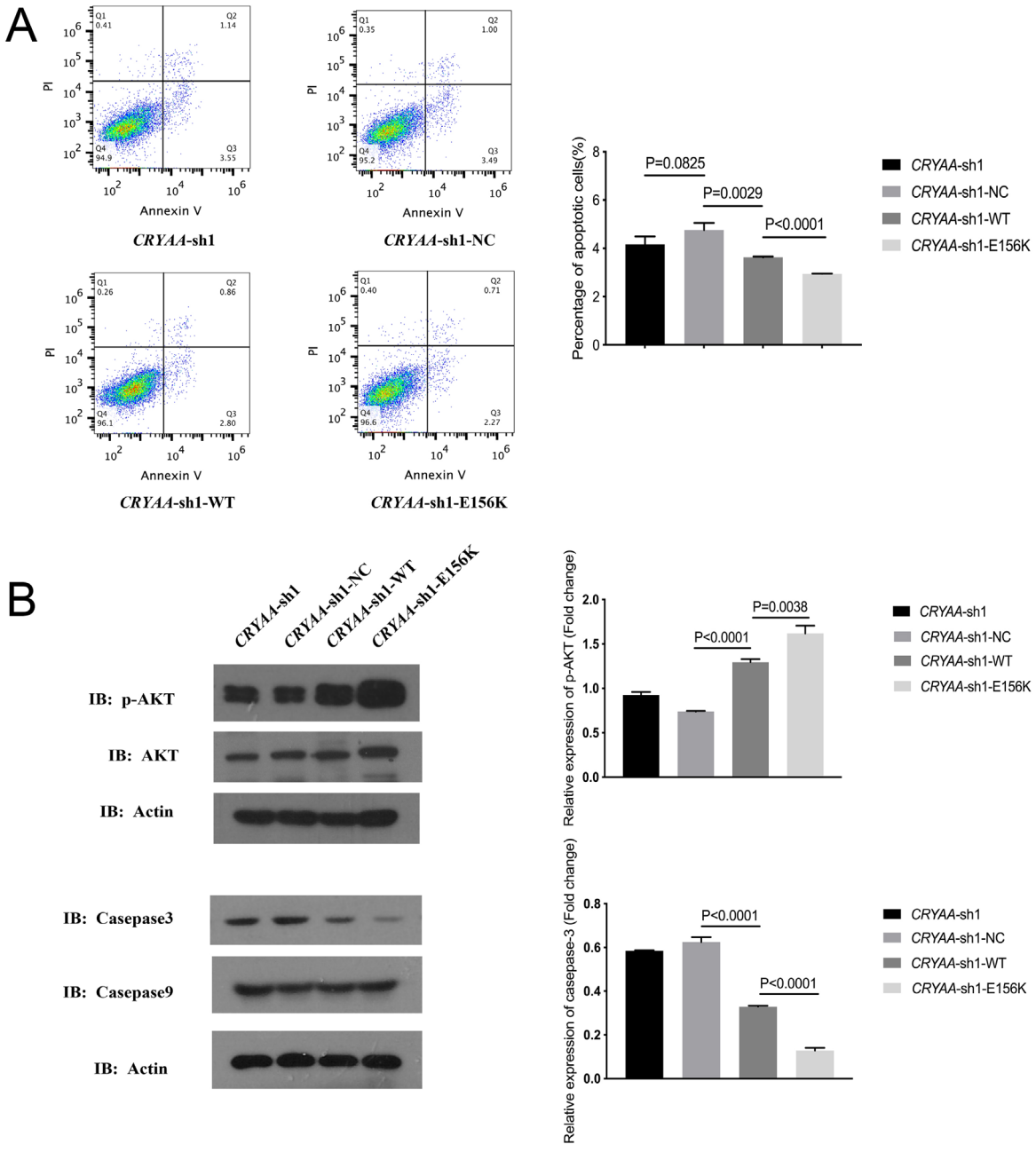

Figure 10. Mutant E156K *CRYAA* decreased cell apoptosis. (A) Annexin V-FITC/propidium-iodide staining was performed to analyze cell apoptosis, and annexin V-negative/propidium iodide-positive cells underwent apoptosis. (B) Western blot assays were used to detect the expression of the AKT, p-AKT, casepase-3, and casepase-9 proteins.

which could be enhanced by E156K mutation. However, it was observed that the difference in apoptosis between the mutant and WT *CRYAA*–expressing cells was very small. Most probably the age-related mutant of αA-crystallin, E156K does not confer a strong impact on anti-apoptotic effects due to weak pathogenicity compared to the α-crystallin mutations in congenital cataracts, such as R116C and R116H [36], and might hold strong pathogenicity. In addition, it is possible that this mutation that can cause subtle changes in anti-apoptotic effects and, in association with other environmental factors, may predispose toward the cataract phenotype [8]. Meanwhile, a significant elevation of the p-AKT signaling pathway and downregulation of caspase-3 were observed in E156K-mutant HLECs. A previous study by Hu et al. suggested that *CRYAA* could regulate caspase-3 or Bax and activate the AKT-signaling pathway to suppress apoptosis induced by oxidative stress [37]. However, Pasupuleti et al. demonstrated that the antiapoptotic function is directly related to the chaperone function [38]. In their study, the anti-apoptotic function of human *CRYAA* was enhanced in R21A mutant protein that showed increased chaperone activity through the promotion of AKT phosphorylation [38]. Consistent with their conclusions, we also found that the mutation of E156K enhanced the chaperone function. Together, we concluded that mutant E156K might increase the anti-apoptotic function of HLECs by enhancing the chaperone activity through the activation of the AKT signaling pathway and the inhibition of caspase-3. However, experimental support for this conclusion is required in further studies.

Some limitations can be identified in our study. First, we only evaluated the chaperone activity of *CRYAA* induced by E156K mutation. However, we did not analyze the association between the enhanced chaperone function of E156K mutant *CRYAA* and other mutant crystallins, such as CRYAB, β- and γ-crystallins, and the chaperone function of the α-crystallin oligomeric complexes with αA to αB subunits in a 3:1 ratio, which should be illustrated in further experiments. In addition, the results showed that the mutant E156K *CRYAA* activated the AKT-signaling pathway and induced anti-apoptotic function in HLECs, while the relation between them was lacking and must be verified in further studies.

In summary, E156K mutation in *CRYAA* did not result in a significant loss of molecular mass and secondary structure of the *CRYAA* protein. However, mutant E156K altered the tertiary structure and enhanced the chaperone function of *CRYAA* by inducing its surface hydrophobicity. Furthermore, we found that among the proteins interacting with *CRYAA* identified by bioinformatics functional analysis, AKT/P-AKT was activated in the mutant E156K group, which seemed to be the possible mechanism underlying the activation of the anti-apoptotic function induced by E156K mutation.

APPENDIX 1. SUPPLEMENTARY FIGURE 1.

To access the data, click or select the words "Appendix 1." Flow cytometric analysis revealed a slight increase of cell percentage in S phase of the cell cycle and a decrease in G2 phase in wild-type and E156K mutant cells. No significant differences were observed between the two groups/

APPENDIX 2. SUPPLEMENTARY FIGURE 2.

To access the data, click or select the words "Appendix 2." CCK8 assay results showed no significant difference in cell proliferation between wild-type and E156K CRYAA.

ACKNOWLEDGMENTS

This study was supported by Shanghai Science and Technology Commission 22 (Scientific Innovation Action Plan, grant no. 20ZR1410100). Dr. Lu (luyieent@126.com) and Dr. Jiang (Yongxiang_Jiang @163.com) are co-corresponding authors for this paper.

REFERENCES

1. Causes of blindness and vision impairment in 2020 and trends over 30 years, and prevalence of avoidable blindness in relation to VISION 2020: the Right to Sight: an analysis for the Global Burden of Disease Study. Lancet Glob Health 2021; 9:e144-60. [PMID: 33275949].

2. Flaxman SR, Bourne RRA, Resnikoff S, Ackland P, Braithwaite T, Cicinelli MV, Das A, Jonas JB, Keeffe J, Kempen JH, Leasher J, Limburg H, Naidoo K, Pesudovs K, Silvester A, Stevens GA, Tahhan N, Wong TY, Taylor HR. Global causes of blindness and distance vision impairment 1990–2020: a systematic review and meta-analysis. Lancet Glob Health 2017; 5:e1221-34. [PMID: 29032195].

3. Brady JP, Garland D, Duglas-Tabor Y, Robison WG Jr, Groome A, Wawrousek EF. Targeted disruption of the mouse alpha A-crystallin gene induces cataract and cytoplasmic inclusion bodies containing the small heat shock protein alpha B-crystallin. Proc Natl Acad Sci USA 1997; 94:884-9. [PMID: 9023351].

4. Su S, Liu P, Zhang H, Li Z, Song Z, Zhang L, Chen S. Proteomic analysis of human age-related nuclear cataracts and normal lens nuclei. Invest Ophthalmol Vis Sci 2011; 52:4182-91. [PMID: 21436267].

5. Zhou P, Luo Y, Liu X, Fan L, Lu Y. Down-regulation and CpG island hypermethylation of CRYAA in age-related nuclear cataract. FASEB J 2012; 26:4897-902. [PMID: 22889833].

6. Liao J, Su X, Chen P, Wang X, Xu L, Li X, Thean L, Tan C, Tan AG, Tay WT, Jun G, Zheng Y, Chew M, Wang YX, Tan

QS, Barathi VA, Klein BE, Saw SM, Vithana EN, Tai ES, Iyengar SK, Mitchell P, Khor CC, Aung T, Wang JJ, Jonas JB, Teo YY, Wong TY, Cheng CY. Meta-analysis of genome-wide association studies in multiethnic Asians identifies two loci for age-related nuclear cataract. Hum Mol Genet 2014; 23:6119-28. [PMID: 24951543].

7. Bhagyalaxmi SG, Padma T, Reddy GB, Reddy KR. Association of G>A transition in exon-1 of alpha crystallin gene in age-related cataracts. Oman J Ophthalmol 2010; 3:7-12. [PMID: 20606865].

8. Bhagyalaxmi SG, Srinivas P, Barton KA, Kumar KR, Vidyavathi M, Petrash JM, Bhanuprakash Reddy G, Padma T. A novel mutation (F71L) in alphaA-crystallin with defective chaperone-like function associated with age-related cataract. Biochim Biophys Acta 2009; 1792:974-81. [PMID: 19595763].

9. Ma X, Jiao X, Ma Z, Hejtmancik JF. Polymorphism rs7278468 is associated with Age-related cataract through decreasing transcriptional activity of the CRYAA promoter. Sci Rep 2016; 6:23206-[PMID: 26984531].

10. Zhao Z, Fan Q, Zhou P, Ye H, Cai L, Lu Y. Association of alpha A-crystallin polymorphisms with susceptibility to nuclear age-related cataract in a Han Chinese population. BMC Ophthalmol 2017; 17:133-[PMID: 28755661].

11. Kumar PA, Haseeb A, Suryanarayana P, Ehtesham NZ, Reddy GB. Elevated expression of alphaA- and alphaB-crystallins in streptozotocin-induced diabetic rat. Arch Biochem Biophys 2005; 444:77-83. [PMID: 16309625].

12. Schrödinger-Release. Schrödinger Release 2017–3. Prime, Schrödinger, LLC, New York, NY 2017.

13. Validandi V, Reddy VS, Srinivas PN, Mueller NH, Bhagyalaxmi SG, Padma T, Petrash JM, Reddy GB. Temperature-dependent structural and functional properties of a mutant (F71L) αA-crystallin: molecular basis for early onset of age-related cataract. FEBS Lett 2011; 585:3884-9. [PMID: 22085609].

14. Li D, Han X, Zhao Z, Lu Y, Yang J. Functional analysis of deleterious EPHA2 SNPs in lens epithelial cells. Mol Vis 2021; 27:384-95. [PMID: 34220184].

15. Bailey TL, Boden M, Buske FA, Frith M, Grant CE, Clementi L, Ren J, Li WW, Noble WS. MEME SUITE: tools for motif discovery and searching. Nucleic Acids Res 2009; 37:W202–208-[PMID: 19458158].

16. Bova MP, Yaron O, Huang Q, Ding L, Haley DA, Stewart PL, Horwitz J. Mutation R120G in alphaB-crystallin, which is linked to a desmin-related myopathy, results in an irregular structure and defective chaperone-like function. Proc Natl Acad Sci USA 1999; 96:6137-42. [PMID: 10339554].

17. Li Z, Hirst JD. Quantitative first principles calculations of protein circular dichroism in the near-ultraviolet. Chem Sci 2017; 8:4318-33. [PMID: 29163925].

18. Fan Q, Huang LZ, Zhu XJ, Zhang KK, Ye HF, Luo Y, Sun XH, Zhou P, Lu Y. Identification of proteins that interact with alpha A-crystallin using a human proteome microarray. Mol Vis 2014; 20:117-24. [PMID: 24453475].

19. Huang W, Sherman BT, Lempicki RA. Bioinformatics enrichment tools: paths toward the comprehensive functional analysis of large gene lists. Nucleic Acids Res 2009; 37:1-13. [PMID: 19033363].

20. Huang W, Sherman BT, Lempicki RA. Systematic and integrative analysis of large gene lists using DAVID bioinformatics resources. Nat Protoc 2009; 4:44-57. [PMID: 19131956].

21. Ito H, Kamei K, Iwamoto I, Inaguma Y, Nohara D, Kato K. Phosphorylation-induced change of the oligomerization state of alpha B-crystallin. J Biol Chem 2001; 276:5346-52. [PMID: 11096101].

22. Laurie KJ, Dave A, Straga T, Souzeau E, Chataway T, Sykes MJ, Casey T, Teo T, Pater J, Craig JE, Sharma S, Burdon KP. Identification of a novel oligomerization disrupting mutation in CRYAA associated with congenital cataract in a South Australian family. Hum Mutat 2013; 34:435-8. [PMID: 23255486].

23. Yang Z, Su D, Li Q, Ma Z, Yang F, Zhu S, Ma XA. R54L mutation of CRYAA associated with autosomal dominant nuclear cataracts in a Chinese family. Curr Eye Res 2013; 38:1221-8. [PMID: 24074001].

24. Kundu M, Sen PC, Das KP. Structure, stability, and chaperone function of alphaA-crystallin: role of N-terminal region. Biopolymers 2007; 86:177-92. [PMID: 17345631].

25. Biswas A, Miller A, Oya-Ito T, Santhoshkumar P, Bhat M, Nagaraj RH. Effect of site-directed mutagenesis of methylglyoxal-modifiable arginine residues on the structure and chaperone function of human alphaA-crystallin. Biochemistry 2006; 45:4569-77. [PMID: 16584192].

26. Sun TX, Das BK, Liang JJ. Conformational and functional differences between recombinant human lens alphaA- and alphaB-crystallin. J Biol Chem 1997; 272:6220-5. [PMID: 9045637].

27. Farnsworth P, Singh K. Structure function relationship among alpha-crystallin related small heat shock proteins. Exp Eye Res 2004; 79:787-94. [PMID: 15655895].

28. Sharma KK, Kumar RS, Kumar GS, Quinn PT. Synthesis and characterization of a peptide identified as a functional element in alphaA-crystallin. J Biol Chem 2000; 275:3767-71. [PMID: 10660525].

29. Kumar RS, Sharma KK. Chaperone-like activity of a synthetic peptide toward oxidized gamma-crystallin. J Pept Res 2000; 56:157-64. [PMID: 11007272].

30. Yan H, Harding JJ, Hui YN, Li MY. Decreased chaperone activity of alpha-crystallin in selenite cataract may result from selenite-induced aggregation. Eye (Lond) 2003; 17:637-45. [PMID: 12855974].

31. Wells-Knecht KJ, Brinkmann E, Wells-Knecht MC, Litchfield JE, Ahmed MU, Reddy S, Zyzak DV, Thorpe SR, Baynes JW. New biomarkers of Maillard reaction damage to proteins. Nephrol Dial Transplant 1996; 11:Suppl 541-7. [PMID: 9044306].

32. Baynes JW. The role of AGEs in aging: causation or correlation. Exp Gerontol 2001; 36:1527-37. [PMID: 11525875].

33. Xi JH, Bai F, Andley UP. Reduced survival of lens epithelial cells in the alphaA-crystallin-knockout mouse. J Cell Sci 2003; 116:1073-85. [PMID: 12584250].

34. Zhou P, Ye HF, Jiang YX, Yang J, Zhu XJ, Sun XH, Luo Y, Dou GR, Wang YS, Lu Y. αA crystallin may protect against geographic atrophy-meta-analysis of cataract vs. cataract surgery for geographic atrophy and experimental studies. PLoS One 2012; 7:e43173-[PMID: 22916220].

35. Liu JP, Schlosser R, Ma WY, Dong Z, Feng H, Lui L, Huang XQ, Liu Y, Li DW. Human alphaA- and alphaB-crystallins prevent UVA-induced apoptosis through regulation of PKCalpha, RAF/MEK/ERK and AKT signaling pathways. Exp Eye Res 2004; 79:393-403. .

36. Kore R, Hedges RA, Oonthonpan L, Santhoshkumar P, Sharma KK, Abraham EC. Quaternary structural parameters of the congenital cataract causing mutants of αA-crystallin. Mol Cell Biochem 2012; 362:93-102. [PMID: 22045060].

37. Hu WF, Gong L, Cao Z, Ma H, Ji W, Deng M, Liu M, Hu XH, Chen P, Yan Q, Chen HG, Liu J, Sun S, Zhang L, Liu JP, Wawrousek E, Li DW. αA- and αB-crystallins interact with caspase-3 and Bax to guard mouse lens development. Curr Mol Med 2012; 12:177-87. [PMID: 22280356].

38. Pasupuleti N, Matsuyama S, Voss O, Doseff AI, Song K, Danielpour D, Nagaraj RH. The anti-apoptotic function of human αA-crystallin is directly related to its chaperone activity. Cell Death Dis 2010; 1:e31-[PMID: 21364639].

Articles are provided courtesy of Emory University and the Zhongshan Ophthalmic Center, Sun Yat-sen University, P.R. China. The print version of this article was created on 1 October 2022. This reflects all typographical corrections and errata to the article through that date. Details of any changes may be found in the online version of the article.